Master

Distribution Category:
LMFBR—Physics
(UC-79d)

ANL-80-104

ARGONNE NATIONAL LABORATORY
9700 South Cass Avenue
Argonne, Illinois 60439

IMPROVED ALGORITHMS FOR THE CALCULATION OF RESOLVED RESONANCE CROSS SECTIONS WITH APPLICATIONS TO THE STRUCTURAL DOPPLER EFFECT IN FAST REACTORS

by

R. N. Hwang, B. J. Toppel,
and H. Henryson II

Applied Physics Division

October 1980

TABLE OF CONTENTS

LIST OF FIGURES

LIST OF TABLES

LIST OF TABLES (Contd.)

IMPROVED ALGORITHMS FOR THE CALCULATION OF RESOLVED RESONANCE CROSS SECTIONS WITH APPLICATIONS TO THE STRUCTURAL DOPPLER EFFECT IN FAST REACTORS

by

R. N. Hwang, B. J. Toppel and H. Henryson II

ABSTRACT

Motivated by a need for an economical yet rigorous tool which can address the computation of the structural material Doppler effect, an extremely efficient improved RABANL capability has been developed utilizing the fact that the Doppler broadened line shape functions become essentially identical to the natural line shape functions or Lorentzian limits beyond about 100 Doppler widths from the resonance energy, or when the natural width exceeds about 200 Doppler widths.

The computational efficiency has been further enhanced by pre-processing or screening a significant number of selected resonances during library preparation into composition and temperature independent "smooth" background cross sections. The resonances which are suitable for such pre-processing are those which are either very broad or those which are very weak. The former contribute very little to the Doppler effect and their self-shielding effect can readily be averaged into slowly varying background cross section data, while the latter contribute very little to either the Doppler or to self-shielding effects.

To illustrate the accuracy and efficiency of the improved RABANL algorithms and resonance screening techniques, calculations have been performed for two systems, the first with a composition typical of the STF converter region and the second typical of ar LMFBR core composition.

Excellent agreement has been found for RABANL compared to the reference Monte Carlo solution obtained using the code VIM, and improved results have also been obtained for the narrow resonance approximation in the ultra-fine-group option of MC^2-2.

I. INTRODUCTION

The rigorous treatment of self-shielded resonance cross sections over a wide energy span generally requires an excessive amount of computing time if a large number of resonances is involved. One of the most time consuming aspects of this problem is the computation of the Doppler broadened line shape functions which are required for each contributing resonance and at each energy point in the calculation.

As a general rule, the choice of the hyper-fine-group (hfg) width (and hence the number of energy points involved in the slowing down calculation) in the rigorous RABANL capability of MC^2-2[1] is based on two criteria. First the hfg width must be small compared to the widths of the individual resonances under consideration to ensure the accuracy of the computed self-shielding and Doppler effects. Secondly the hfg width must also be small compared to the maximum lethargy increment due to scattering by the heaviest isotope in the mixture in order to accurately account for the Placzek oscillations.[2] These two considerations lead to extremely narrow hfg and hence to a very large number of energy points in the calculation, especially if a large energy is to be spanned. The utility of RABANL for various applications may therefore be seriously impacted especially as more resolved resonance data become available.

The problem is well illustrated by current design calculations for the STF.[3,4] In contrast to the usual fast breeder reactor, the Doppler effect in the converter region of the STF depends almost entirely upon the Fe, Cr, and Ni constituents of stainless steel due to the unusually high concentration of that material in the design. Hence an accurate calculation of the resonance cross sections of these medium weight nuclei is essential.

The resolved resonances for the STF system span an energy of the order of 655 keV and approximately 2×10^5 RABANL hfg are involved in the slowing down calculation. There may be as many as 1500 resolved resonances in the mixture, each of which contributes to the cross sections at each of the hfg.

On the order of 2.6×10^8 Doppler broadened line shapes must be evaluated if RABANL is used in a straightforward manner. Even using the extremely fast MC^2-2 bivariate table interpolation routine QUICKW[1] to obtain the Doppler broadened line shapes, over 40 minutes of IBM 370/195 time is required just in calculating the resonance cross sections.

About half of the resonances involved in the STF calculation belong to the medium weight nuclei. The cross sections of these nuclei are characterized by the presence of extremely wide s-wave resonances with natural widths on the order of several keV, and relatively sharp p-wave resonances. The latter are the main contributors to the Doppler effect. These characteristics give rise to various difficulties for all of the existing methods which are designed primarily for the low lying resonances of the heavy absorbers. In particular, the narrow resonance (NR)

approximation used in the MC^2-2 ultra-fine-group (ufg) option becomes dubious for the wide structural resonances especially if the resonance integrals are evaluated over the entire energy range.

Motivated by the need for an economical yet rigorous computational tool which can address structural material resonances, extensive work has been carried out to improve the efficiency of the RABANL capability in MC^2-2.

An obvious improvement can be made by tailoring the algorithm with regard to the contribution from the tails of distant resonances. The efficiency can be further enhanced by preprocessing the resonance data so that fewer resonances need be treated by RABANL.

An exceedingly efficient improved RABANL capability and a time saving data preprocessing procedure have been developed and are described in Section II. Since there may be of the order of 100 times as many hfg as ufg in a typical MC^2-2 problem,[1] the ufg NR approximation option provides an attractive economical approximation to the rigorous RABANL option. The data preprocessing has been found to provide an ancillary benefit in that the NR ufg approximation of MC^2-2 has become more reliable and now produces more accurate cross sections.

Numerical results are presented in Section III for two systems; one is typical of a fast breeder reactor core and the other typical of the STF converter region. The results of the new algorithms and data preprocessing are compared with the original MC^2-2 methods and with results using the Monte Carlo reference code VIM.[5,6]

II. RABANL ALGORITHM IMPROVEMENTS AND RESONANCE DATA PREPROCESSING

A. RABANL Algorithm Improvements

The efficiency of RABANL can be improved dramatically if the detailed computation of the Doppler broadened line shape functions of distant resonances and of extremely wide resonances can be significantly reduced. This has been achieved without sacrificing the required accuracy by utilizing the asymptotic behaviour of these functions in conjunction with the ultra-fine-group structure of MC^2-2.[1]

In particular, in the limit when either x or ξ is large, the symmetric and antisymmetric Doppler broadened line shape functions become

$$\psi(\xi, x) = \frac{\xi\sqrt{\pi}}{2} \operatorname{ReW}\left(\frac{x\xi}{2}, \frac{\xi}{2}\right) \approx \frac{1}{1+x^2}\left[1 + \frac{1}{\xi^2} \cdot \frac{6x^2 - 2}{(1+x^2)^2} + \ldots\right] , \tag{1}$$

and

$$\chi(x, \xi) = \xi\sqrt{\pi} \operatorname{ImW}\left(\frac{x\xi}{2}, \frac{\xi}{2}\right) \approx \frac{2x}{1+x^2}\left[1 + \frac{1}{\xi^2} \cdot \frac{2x^2 - 6}{(1+x^2)^2} + \ldots\right] , \tag{2}$$

respectively, where

$$\xi = \frac{\Gamma_t}{\Delta}$$

Γ_t = the total line width

$\Delta = \left(\frac{4kTE}{A}\right)^{1/2}$, the Doppler width

k = the Boltzmann constant, 8.6168×10^{-5} eV/degree Kelvin
T = the temperature in degrees Kelvin
E = the laboratory neutron energy in eV
A = the ratio of the mass of the target resonance isotope to the mass of the neutron

W(z) = the Dawson integral with complex arguments
= $\exp(-z^2)\ \operatorname{erfc}(-iz)$ where $z = x + iy$

$$x = \frac{2(E - E_o)}{\Gamma_t}$$

E_o = the resonance energy in eV.

When $|x\xi/2| = |E - E_o|/\Delta > 100$ or $\xi/2 = \Gamma_t/2\Delta > 100$ the second order terms in Eqs. 1 and 2 become several thousand times smaller than the leading terms and can hence be ignored. Under this condition the temperature independent natural line shape (or Lorentzian) functions

$$\psi \approx \frac{1}{1 + x^2} \tag{3}$$

and

$$\chi \approx \frac{2x}{1 + x^2} \tag{4}$$

can be used.

For realistic problems at or above room temperature, beyond the above limits the shelf-shielding effect of the resonance under consideration is generally insignificant at the hfg level. Also the ψ function is either vanishingly small or smoothly varying, and the χ function always varies slowly within reasonably small energy intervals. In particular, under the above condition, for the ultra-fine-group (ufg) width currently used in MC^2-2 ($\Delta u = 0.00833$), these asymptotic functions can be adequately represented by their averaged values within the ufg, namely

$$\frac{1}{\Delta x}\int_{x_{i+1}}^{x_i} \psi \, dx = \frac{1}{\Delta x}\left[\arctan x_i - \arctan x_{i+1}\right] \approx \frac{1}{\bar{x}^2 + 1} \tag{5}$$

and

$$\frac{1}{\Delta x}\int_{x_{i+1}}^{x_i} \chi \, dx = \frac{1}{\Delta x} \ln \frac{1 + x_i^2}{1 + x_{i+1}^2} \approx \frac{2\bar{x}}{\bar{x}^2 + 1} \tag{6}$$

where Δx is $x_i - x_{i+1}$, x_i and x_{i+1} correspond to the values at the ufg boundaries, and $\bar{x}$ is taken at the midpoint of the ufg. Resonances lying outside the ufg and having both $x\xi/2$ and $|\xi/2|$ less than or equal to 100 are treated explicitly for each hfg. The Doppler width in ξ uses the highest temperature for the material involved, in any composition in which that material occurs, and is evaluated for an energy corresponding to the midpoint of the ufg. The E in x correspond to the energy at the edge of the ufg closest to the resonance in question.

Resonances lying outside the group which have either $|x\xi/2| > 100$ or $\xi/2 > 100$ and for which the ratio of natural line width to ufg width is greater than four, assume the averaged values based on the Lorentzian shapes as given in Eqs. 5 and 6. These averaged values are then assigned to all hfg lying within that ufg.

Both $|x\xi/2|$ and $\xi/2$ may exceed 100 even for narrow resonances, for example at extremely low temperatures. To ensure the accuracy of the self-shielding calculation for such narrow resonances which may fail the above criteria, a further test is made on R, the ratio of the separation of the resonance from the ufg, to the natural width. For nuclei of mass less than 91 (which are characterized by relatively wide resonances lying relatively high in energy where the self-shielding effect is less important) R is taken to be three. For nuclei of mass greater than or equal to 91 (which are characterized by sharp low lying resonances with extremely large self-shielding effect) R is taken to be 10. If R exceeds the appropriate value according to the mass of the resonance material, the averaged values are used for all hfg in the ufg. In all other cases, the resonance in question contributes explicitly to each hfg in the ufg using the Doppler broadened line shape functions.

This approach greatly minimizes the number of times that the Doppler broadened line shape functions must be obtained and more than a factor of eight reduction in execution time has been achieved compared with the original algorithm.

Numerical examples will be given in Section III.

B. Resonance Data Preprocessing

Computational efficiency in RABANL can obviously be further enhanced if a significant number of the resolved resonances in the problem can be eliminated by virtue of having been preprocessed during the preparation of the MC^2-2 library into composition and temperature independent ufg "smooth" cross sections. Any resonances which are to be preprocessed must obviously make a negligible contribution to the overall Doppler effect and must be adequately self-shielded at the ufg level in order to preserve the accuracy of the calculation.

Resolved resonances can be characterized as belonging to one of two types. The first are the extremely wide resonances with natural widths much larger than both the corresponding Doppler width and the ufg width. Large Γ_t/Δ ensures temperature independence and large resonance width compared to the ufg width ensures the adequacy of the ufg structure to represent the energy details of the resonance. Such resonances are hence suitable for preprocessing.

The second type of resonance is typified by the extremely weak resonances belonging to the medium weight nuclei of low natural abundance, or some extremely weak p-wave resonances of the heavy nuclei of low natural abundance. These resonances normally contribute very little to either the overall Doppler effect or to the self-shielding effect and hence may also be suitable for preprocessing.

The logic used to screen the resonances to determine which can be preprocessed into "smooth" cross sections, which will be retained, and which are candidates for elimination based on subsequent tests is shown in Fig. 1. The adequacy of this logic is demonstrated in the numerical examples given in Section III.

The "WIDTH" in Fig. 1 is the larger of the natural width Γ_t, or the Doppler width Δ evaluated at a temperature of 300 degrees Kelvin, and ξ is Γ_t/Δ as before.

Resonances having widths corresponding to two or more ultra fine groups and having $\Gamma_t \geq 50\ \Delta$ fall into the first type described above and are eliminated by means of preprocessing. For nuclei with mass less than 91, the above conditions can be relaxed. For these nuclei the Doppler effect depends almost entirely on the sharp p-wave resonances. Also, the s-wave resonances having widths somewhat less than two ufg can be treated at the ufg level without appreciable loss of accuracy. This has been well demonstrated by such codes as ELMOE[7] and MC$^{2(8)}$ for sodium and the structural materials, for example. Hence resonances of materials of mass less than 91 and with widths corresponding to one or more ultra-fine-groups are also eliminated by means of preprocessing if the resonance energy E_o is greater than 10 keV and $\Gamma_t \geq 25\Delta$, or if $E_o \leq 10$ keV and $\Gamma_t \geq 10\ \Delta$ respectively.

The relaxed criteria for mass less than 91 are important from a practical point of view in that they permit elimination of most of the low lying resonances of Mn^{55} with exceedingly large peak cross sections. The benefit of eliminating the relatively wide resonances will be further discussed in the next section.

Resonances for materials of mass greater than or equal to 91 having widths greater than or equal to two ufg but having $\xi \leq 50$ are further examined as to their contribution to the overall Doppler effect. This procedure is described in detail below.

Resonances failing the above criteria may fall into the second class described above and a more elaborate set of tests is required to examine the self-shielding and Doppler characteristics of the individual resonances involved. These are described next.

A convenient procedure is to utilize the NR approximation to the individual resonance integrals which are characterized by two parameters, namely β_k and ξ_k. ξ_k has been defined earlier and β_k is the ratio of the macroscopic smooth background cross section to the macroscopic peak cross section of resonance k. To be conservative, β_k is calculated using only the natural abundances of the isotopes of the material having resonance k. Thus resonance k appears to be more heavily self-shielded than it would be in the more dilute realistic mixture.

In order to qualify as a candidate for preprocessing, the weak resonance k is required to satisfy two criteria: (1) the difference between the infinitely dilute and self-shielded resonance integrals for resonance k must be small compared to the sum of the self-shielded resonance integrals for the other resonances of the same material lying within an energy span comparable to or smaller than the typical broad group (bg) width; (2) the derivative of the self-shielding factor (the ratio of self-shielded to infinitely dilute resonance integrals) with respect to Δ_k for resonance k must be small compared to the sum of the derivatives of all neighboring

resonances of the same material lying within the selected energy span. After the candidates are chosen, the final selection of the resonances to be preprocessed are chosen from among the candidates as indicated later. The algorithm used is described in detail below.

For the present purpose, the exact evaluation of the self-shielding factor is unnecessary. One convenient way to estimate the relative importance of the self-shielding effect and the Doppler effect for a particular resonance is to examine the self-shielding factor, F_k, under two extreme conditions, namely

$$F_k = \left(\frac{\beta_k}{\beta_k + 1}\right)^{1/2} \tag{7}$$

or

$$F_k = \frac{\beta_k}{\beta_k + \rho_k} \tag{8}$$

Equation 7 represents the zero broadening (zero temperature) limit and Eq. 8 is the extreme broadening or large β (high dilution) limit.[9] ρ_k is defined by

$$\rho_k = \frac{1}{2}\psi_k(\sqrt{2}\,\xi_k,\ 0) = \frac{\sqrt{\pi}}{2\sqrt{2}}\,\xi_k e^{\frac{\xi_k^2}{2}}\ \mathrm{erfc}\ \left(\frac{\xi_k}{\sqrt{2}}\right) \tag{9}$$

and the Doppler width in ξ_k is evaluated at the resonance energy using a temperature of 300°K. To be conservative, the smaller of the values obtained from Eqs. 7 and 8 is used for the self-shielding factor. It should be noted that Eq. 8 is practically exact for the weak resonances which will be eliminated by means of preprocessing.

A convenient upper limit for the derivative of the self-shielding factor with respect to Δ_k is obtained using

$$D_k = \frac{d}{d\Delta_k}\left(\frac{\beta_k}{\beta_k + \rho_k}\right) = \frac{\beta_k}{(\beta_k + \rho_k)^2}\,\frac{\partial \xi_k}{\partial \Delta_k}\,\frac{d\rho_k}{d\xi_k} \tag{10}$$

and using Eq. 9 to obtain the last factor. Based on numerical studies, it was found to be conservative to obtain D_k using a temperature of 300°K for materials of mass greater than or equal to 91 and 2000°K for materials of mass less than 91.

The energy spanned by all of the resonances of the material is broken up into lethargy intervals of 0.25 starting at the energy of the highest resolved resonance. Each interval starts at the energy of the highest resolved resonance in that interval. Within each energy the sums

$$S_F = \sum_k F_k/\beta_k \tag{11}$$

$$S_D = \sum_k D_k/\beta_k \tag{12}$$

are computed and then the relative contribution of each resonance to the self-shielding effect and to the temperature derivative,

$$R_{F_K} = \frac{1 - F_k}{\beta_k S_F} \tag{13}$$

$$R_{D_K} = \frac{D_k}{\beta_k S_D} \tag{14}$$

are obtained.

In Fig. 1, DOPPLER < 0.01 implies R_{D_K} given in Eq. 14 is less than 0.01 and SELF-SHIELDING < 0.01 implies R_{F_K} given in Eq.13 is less than 0.01. Only the extremely weak resonances can pass these two tests simultaneously. To preserve the magnitudes of the broad group cross sections, the contributions from these screened-out resonances are then incorporated into the ufg composition independent "smooth" cross sections when the base library is prepared.

C. Improvements in NR Approximation Accuracy

Apart from the obvious improvement in computing efficiency, the resolved resonance data preprocessing provides the ancillary benefit of making the NR approximation used in the ufg treatment of MC^2-2 valid in the presence of the medium weight nuclei. The NR approximation can be further improved by (1) modification of the conventional NR treatment of the resonance integral as described in Ref. 10, and (2) modification of the subsequent continuous slowing down treatment. The former requires the correction which accounts for the effect of Placzek oscillations on the resonance integral due to the resonance under consideration. The latter requires knowledge of the short range fluctuations which resonances at higher energies produce in the collision density in addition to the conventional attenuation approach based on the Wigner approximation. These can be accomplished readily if the Placzek oscillations are accounted for only in the first collision lethargy interval.

The Placzek correction to the resonance integral is defined as[10]

$$\tilde{J}_x = J^*_x \cdot [2 - \frac{1}{\theta_r}(1 - e^{-\theta_r})] \tag{15}$$

where

$$\theta_r = \frac{J^*_s}{1 - \alpha_r} - QJ^*_t \tag{16}$$

$$Q = \sum_i \frac{1}{1-\alpha_i} \frac{\Sigma_{si}^b}{\Sigma_t^b} \tag{17}$$

$$\alpha_i = \frac{(A_i-1)^2}{(A_i+1)^2} \tag{18}$$

and x designates capture, fission, scattering or total.

Two necessary conditions for the validity of Eq. 15 are: (1) the extent of the resonance must be small compared to the maximum energy loss per collision; (2) the quantity defined in the square bracket of Eq. 15 must be greater than zero. The latter condition requires that $\theta_r \gtrsim -1.25$. To ensure that these conditions are satisfied, Eq. 15 will be used only for resonances with resonance energy $E_0 > 50$ eV and $\theta_r > -1.0$. It should also be noted that, strictly speaking, Eq. 15 is correct for resonance integrals dominated by the J-integral component without the interference terms. This is usually true for the relatively high energy region where the approximation is applicable.

The improved NR treatment is practically exact for the p-wave resonances of structural isotopes which remain after the preprocessing. The elimination of wider resonances in conjunction with the improved NR approximation generally provides improved accuracy especially when the Doppler effect is considered. Below about 200eV however, the method must be expected to deteriorate due to the gradual break down of the basic assumptions.

For the weighting spectrum calculations, the correction to the Placzek oscillations in the first collision interval is taken to be a simple step function with magnitude of e^{θ_r} and width of C_r, the maximum lethargy increment per collision. This correction has been incorporated into the continuous slowing down method of the MC^2-2 code.

III. RESULTS AND DISCUSSIONS

To illustrate and validate various improvements described in the preceeding section, extensive calculations have been carried out for two distinct systems typical of an STF converter and an LMFBR composition. The isotopic concentrations of these systems are given in Tables I and II respectively. Table III shows the broad group structure used in the calculations and the resolved resonance energy ranges for the six most important nuclides with respect to this group structure. The upper energy for the RABANL calculations was taken to be 150 keV and ENDF/B-IV data were used in all the calculations. For the sake of simplicity, only the homogeneous option in RABANL was considered.

The difficulties in the rigorous treatment of self-shielded resonance cross sections in a typical LMFBR calculation using the RABANL option can be best illustrated by some actual statistics as given in Table IV. To cover an energy span of 150 keV, the total number of hfg required and the total number of resonances involved are exceedingly large. These numbers can increase dramatically if all the resolved resonances of the medium weight nuclides up to 650 keV are also accounted for. For comparison, the total number of hfg and resonances for energy spans of 4 keV and 300 eV, which correspond to the resolved energy ranges for ^{238}U and ^{239}Pu respectively, are also given. The total number of hfg indicated here was based on the smaller of 4 hfg per minimum Doppler width in a broad group or 10 hfg per maximum lethargy increment per collision for the heaviest nuclides in the system. This default criterion was found to be adequate although the number of hfg can be specified by the user. Once the total number of hfg is fixed, the CPU time requirement will be determined by: (1) the efficiency of the algorithm in treating the contributions from tails of all distant resonances and (2) the total number of resonances to be treated.

A. Algorithm Improvements

Tables V and VI show the capture cross sections of Fe, Cr, Ni, and ^{238}U, and the fission cross sections of ^{235}U for the STF converter at 300°K as obtained by the original exact algorithm and the improved algorithm, respectively. Total cross sections for the main structural materials are given in Table VII. All resonances below 150 keV were included in the calculations. It is quite evident from these results that the cross sections remain practically unchanged when the exact treatment is replaced by the improved treatment for the distant resonances. Since the new method is used only for those resonance tails which have already assumed the Lorentzian shape, the Doppler changes in cross sections obtained by these two methods are also expected to be in good agreement.

In Table VIII, the computational efficiencies of these methods are compared. The CPU time required for the resonance calculations in the original algorithm, which amounts to almost 93 percent of the total CPU time, is reduced by more than a factor of 8 if the improved algorithm is used. Furthermore, the CPU time required for the resonance calculations

becomes comparable to that for other parts of the MC^2-2 code. The significant improvement in efficiency will undoubtedly make the utility of RABANL more attractive in various applications especially for heterogeneous cell calculations where the excessive computing time requirement has always been a serious handicap.

B. Resonance Data Preprocessing

As mentioned earlier, the computational efficiency in RABANL can be further enhanced if the preprocessing scheme is used to minimize the number of resonances in the problem. The validity of this scheme has been examined.

Table IX through Table XVI show the results of $\tilde{\sigma}_\gamma$, and the Doppler changes $\Delta\tilde{\sigma}_\gamma$ obtained with and without resonance data preprocessing for the five main constituents of the STF core converter and for a typical LMFBR composition respectively. For convenience, $\tilde{\sigma}_\gamma$ of the medium weight nuclides and all $\Delta\tilde{\sigma}_\gamma$ are scaled up by 10^3 and 10^6 respectively.

For $\tilde{\sigma}_\gamma$, the results with "screened" resonances are essentially the same as those without screening. The values for $\Delta\tilde{\sigma}_\gamma$ and $\Delta\tilde{\sigma}_f$ are also in good agreement. The only noticeable differences in $\Delta\tilde{\sigma}_\gamma$ were observed in the groups 11 and 12 of relatively high energy. The discrepancies of $\Delta\tilde{\sigma}_\gamma$ for Cr in group 11 are believed to be of little practical importance in the overall Doppler effect of Cr which is dominated by the sharp p-wave resonance in group 18. Furthermore, Cr generally plays a far less important role than Fe in the Doppler effect for structural materials of practical interest.

Figures 2 through 7 illustrate the individual components of the Doppler coefficient due to each nuclide as a function of energy and their contributions to the overall Doppler coefficients in the STF and LMFBR systems respectively. The structural Doppler effect is dominated by Fe in group 19 where the sharp p wave resonance at 1.15 keV occurs. The Cr Doppler coefficient is practically determined by groups 18 and 13 where the agreement in $\Delta\tilde{\sigma}_\gamma$ between the screened and unscreened results is excellent. The unique characteristics of the structural Doppler effect are clearly illustrated in these figures.

The improvement in computational efficiency as the result of the preprocessing scheme is illustrated in Table XVII for the two systems considered. It is interesting to note that the CPU time required for the resonance calculations becomes comparable to that required for other parts of the MC^2-2 code if both the improved algorithm and the preprocessing scheme are used. From Table IV, it is clear that elimination of a large number of resonances of the structural materials above 4 keV, the upper bound for the resolved region of ^{238}U, is primarily responsible for the improved efficiency shown in Table XVII. For heavy nuclides with relatively low lying resolved resonances, the preprocessing scheme has much less of an impact on computing time simply because a much smaller number of resonances can meet the screening criteria.

As discussed in the preceeding section, one ancillary benefit of resolved resonance data preprocessing is to make the NR-approximation much more viable in the presence of medium weight nuclei. Another obvious benefit is to remove the ambiguity concerning the treatment of the closely spaced

unresolved resonances of heavy nuclides within the energy interval where an exceedingly wide resolved resonance of medium weight nuclei occurs. Since the width of the wide resonance may be many times greater than the average level spacing of the unresolved resonances, its effect on the unresolved cross section must be deterministic and not probablistic. It is, therefore, physically more reasonable when the wide resonances are treated as "smooth" cross section on the ufg level in so far as the treatment of the unresolved resonance self-shielding effect is concerned.

C. Improved NR-Algorithm

Further improvement in the NR-approximation in MC^2-2 will provide a faster alternative to RABANL for routine calculations where less rigor is required. Calculations using the improved NR algorithm have been carried out for various cases and, for the purpose of comparison, the same calculations have also been repeated using the VIM Monte Carlo code, RABANL option, and the original NR-approach without corrections. Results of these calculations are summarized in Tables XVIII through XXVII. Unlike the previous cases, the unresolved resonance contributions are accounted for in the calculations. Quantities tabulated are the broad group cross sections $\tilde{\sigma}_\gamma$ and $\tilde{\sigma}_t$ at 300°K and the Doppler change $\Delta\tilde{\sigma}_\gamma$. It is important to realize that the impact of the improved NR approximation on each individual resonance integral alone may not automatically improve the values in $\tilde{\sigma}_x$ and $\Delta\tilde{\sigma}_x$. Two other factors that also impact the outcome of $\tilde{\sigma}_x$ and $\Delta\tilde{\sigma}_x$ are: (1) the accuracy of the weighting spectrum used to weight those resonance integrals; (2) group boundary effects.

In the improved NR-approach, the usual continuous slowing down method for obtaining the weighting spectrum was modified to account for the fluctuation in collision density within the first collision interval as described in the last section. Strictly speaking, however, the method cannot account for the detailed behavior of collision density in energy and temperature especially when many resonances are considered. As a general rule, $\tilde{\sigma}_x$ and $\Delta\tilde{\sigma}_x$ are relatively insensitive to the weighting spectrum in the high energy region and become more sensitive as energy decreases. The fact that the inaccuracies in the resonance integral approximations may sometimes be compensated by those in the approximations of weighting spectrum makes comparison of results of the NRA and the improved NRA to those of RABANL difficult to assess particularly when $\Delta\tilde{\sigma}_\gamma$ is considered. The group boundary effect arises from the fact that the limits of integration for each resonance integral extend from $-\infty$ to $+\infty$ independent of the broad group boundaries whereas the resonance integral is assigned to the broad group within which the resonance energy lies. Even though the broad group assignment should not affect the overall reaction rates, the accuracy of the individual broad group $\tilde{\sigma}_x$ and $\Delta\tilde{\sigma}_x$ determined this way becomes difficult to estimate when compared to those obtained by the rigorous RABANL method where the group boundaries are accounted for explicitly. Fortunately, the boundary effect is unimportant for heavy nuclides such as ^{238}U in the relatively high energy region of interest for fast reactor calculations where a broad group usually contains a large number of resonances.

Qualitatively, the improved NRA is at its best when well isolated sharp resonances are considered. For the STF system where the Doppler effect is dominated by a few p-wave resonances in the low keV region, the improved NRA appears to be particularly attractive. This can be illustrated by the results given in Table XVIII through Table XXII. $\tilde{\sigma}_\gamma$ and $\Delta\tilde{\sigma}_\gamma$ are characterized by the existence of a dominant p-wave resonance of Fe at 1.15 keV (group 19) and a dominant p-wave resonance of Cr at 1.626 keV (group 18). Both these resonances are located far away from the broad group boundaries described in Table III. The improvement in $\tilde{\sigma}_\gamma$ and $\Delta\tilde{\sigma}_\gamma$ for these groups is quite obvious. In the higher energy groups, the results obtained by the NRA and the improved NRA become identical as the effect of Placzek oscillations becomes negligible. The discrepancies in $\Delta\tilde{\sigma}_\gamma$ of Cr and Ni between RABANL and the NRA in the high energy groups illustrate the group boundary effect described earlier.

Similar results for the LMFBR system are given in Table XXIII through Table XXVII. By and large, the results obtained by the improved NRA also show better agreement with RABANL than those obtained by the NRA without corrections. There are exceptions, however. For instance, the $\Delta\tilde{\sigma}_\gamma$ for ^{238}U in groups 17 and 18 based on the NRA appear to be slightly better than those based on the improved NRA. Even though such small differences have no practical importance, some discussion is warranted. The behavior is believed to be attributed to the cancellation of errors which can be illustrated by breaking $\Delta\tilde{\sigma}_x$ into two components. By definition,

$$\Delta\tilde{\sigma}_x = \Delta \frac{R_x}{\tilde{\phi}} \approx \frac{\Delta R_x}{\tilde{\phi}} - \tilde{\sigma}_x \frac{\Delta\tilde{\phi}}{\tilde{\phi}} \tag{19}$$

where the first term is the contribution from the Doppler change in reaction rate and the second term is that due to the Doppler change in the average flux. For relatively high energy groups where the overall absorption probabilities are small, the former is primarily determined by the Doppler changes in resonance integrals while the latter in addition is sensitive to the accuracy of the detailed temperature behavior of the weighting spectrum. Thus, the accuracy of the first term reflects the accuracy of the Doppler change in resonance integrals and the accuracy of the second term reflects, at least in part, the accuracy of the temperature behavior in the weighting spectrum. Table XXVIII shows the magnitude of each component and the averaged group flux $\tilde{\phi}$ at the reference temperature as obtained by various methods for groups 17 and 18 in the LMFBR system. The $\tilde{\phi}$'s at the reference temperature are in good agreement for all cases. The agreement means that the Doppler changes in the resonances integrals are weighted properly in both NRA methods for these two groups. $\frac{\Delta R_\gamma}{\tilde{\phi}}$ obtained by the improved NRA are consistently in better agreement with RABANL results than those obtained by the NRA without correction independent of the temperature ranges considered. For the temperature range 774°K-300°K, $-\tilde{\sigma}_\gamma \frac{\Delta\tilde{\sigma}}{\tilde{\sigma}}$ obtained by the improved NRA are

also are in better agreement with the RABANL results. For the temperature range 2000°K-774°K, comparable discrepancies in the latter quantity are observed in both NRA methods as compared to RABANL. It is interesting to note that the underestimation of the reaction rate component in the original NRA is nearly compensated by the overestimation of the flux component. This explains the unexpected trend in $\Delta\tilde{\sigma}_\gamma$ for these groups. The effect of compensating errors can be further illustrated by the similar results given in Table XXIX for the STF system. With the exception of the negligible contribution from ^{238}U at low concentration, the single Fe resonance at 1.15 keV in group 19 is practically isolated. Unlike the $\Delta\phi$ term, the reaction rate component is nearly independent of the temperature behavior of the weighting spectrum. The excellent agreement in $\frac{\Delta R}{\tilde{\phi}}$ between the improved NRA and the RABANL results implies an equally good agreement in the Doppler changes in the resonance integral. Again, the $-\tilde{\sigma}_\gamma \frac{\Delta\tilde{\phi}}{\tilde{\phi}}$ term obtained by the improved NRA also shows better agreement with that of RABANL in the temperature range 774°K-300°K. In the higher temperature range the discrepancies in the latter quantity becomes more noticeable. Comparison of the results of the NRA without correction to those of RABANL indicates that the discrepancies in these components can either be compensative or accumulative.

For lower energy groups, the question of the validity of the improved NRA and the subsequent continuous slowing down approximation become intertwined. It is further complicated by the group boundary effect. All approximate methods based on the narrow resonance assumption eventually break down for groups below about 50 eV and $\Delta\tilde{\sigma}_x$ usually become meaningless for systems with high ^{238}U or ^{232}Th concentrations at these low energies. Hence, the rigorous but efficient RABANL option provides an excellent alternative for the analyst if accuracy in the low energy groups is required.

IV. CONCLUSIONS

It has been shown in the preceeding section that the computational efficiency of the rigorous RABANL capability can be improved dramatically if the improved algorithm is used. The improvement makes possible the utility of the rigorous RABANL option to problems such as structural Doppler effect where an exceedingly large number of resonances span a large energy range. It will undoubtedly also impact the cell heterogeneity calculations where the computing time requirement has always been a primary consideration.

The computational efficiency can be further enhanced by preprocessing or screening a significant number of selected resonances during the library preparation into composition independent "smooth" background ufg cross sections. Criteria are chosen to ensure the preservation of the self-shielding effect and Doppler effect. The scheme is particularly effective for nuclides of medium weight in which a large number of weak and wide resonances are present. For heavy nuclides, few resonances can meet the preprocessing criteria. Apart from the improvement in computing efficiency, the data preprocessing also provides some ancillary benefits. In the absence of the extremely wide resolved resonances, the NR-approximation option in MC^2-2 becomes more viable and the choice of σ_p in the treatment of unresolved resonances becomes much less ambiguous.

In spite of improved efficiency in the RABANL capability, the NR-approximation option in MC^2-2 still plays an important role in routine calculations where less rigor is required. The improvement in the NR-approximation provides such an alternative with both speed and adequate accuracy for typical fast reactor calculations.

REFERENCES

1. H. Henryson, II, B. J. Toppel and C. G. Stenberg, "MC^2-2: A Code to Calculate Fast Neutron Spectra and Multigroup Cross Sections," ANL-8144 (ENDF 239) (June 1976).

2. G. Placzek, "On the Theory of the Slowing Down of Neutrons in Heavy Substances," Phys. Rev. 69, 423 (1946).

3. R. A. Lewis, D. C. Rardin, A. Travelli, J. L. Snelgrove, R. G. Matlock, B. C. Cerutti, K. P. Coover, R. L. Knawa, J. E. Matos, F. D. McCuaig, D. Ramaswami, F. A. Rough, and R. C. Watson, "STF Design Features and Estimated Performance," Trans. International Meeting of Fast Reactor Safety and Related Physics, Chicago, Ill. Oct. 5-8, 1976.

4. A. Travelli, J. E. Matos, J. L. Snelgrove, and R. A. Lewis, "Nuclear Characteristics of the Safety Test Facility (STF) Conceptual Design," Trans. Am. Nucl. Soc. 24, 284 (1976).

5. "Monte Carlo Code Development at Argonne National Laboratory," Proc. of the NEACRP of a Monte Carlo Study Group, ANL-75-2, NEA-CRP-L-1 18, July 1-3, 1974.

6. R. E. Prael, "Cross Section Preparation for the Continuous-Energy Monte Carlo Code VIM," Proc. Conf. on Nuclear Cross Sections and Technology, NBS SP 425, p. 447, Washington, D. C., March 3-7, 1975.

7. A. L. Rago and H. H. Hummel, "ELMOE: An IBM-704 Program Treating Elastic Scattering Resonances in Fast Reactors," ANL-6805 (Jan. 1964).

8. B. J. Toppel, A. L. Rago, and D. M. O'Shea, "MC^2, A Code to Calculate Multigroup Cross Sections," ANL-7318 (June 1976).

9. R. N. Hwang, "Efficient Methods for the Treatment of Resonance Cross Sections," Nucl. Sci. Eng., 52, 157 (1973).

10. R. N. Hwang, "Effect of the Fluctuations in Collision Density on Fast-Reactor Doppler Effect Calculations," Proc. Conf. on Safety, Fuels, and Core Design and Large Fast Power Reactors, ANL-7120, October 11-14, 1965.

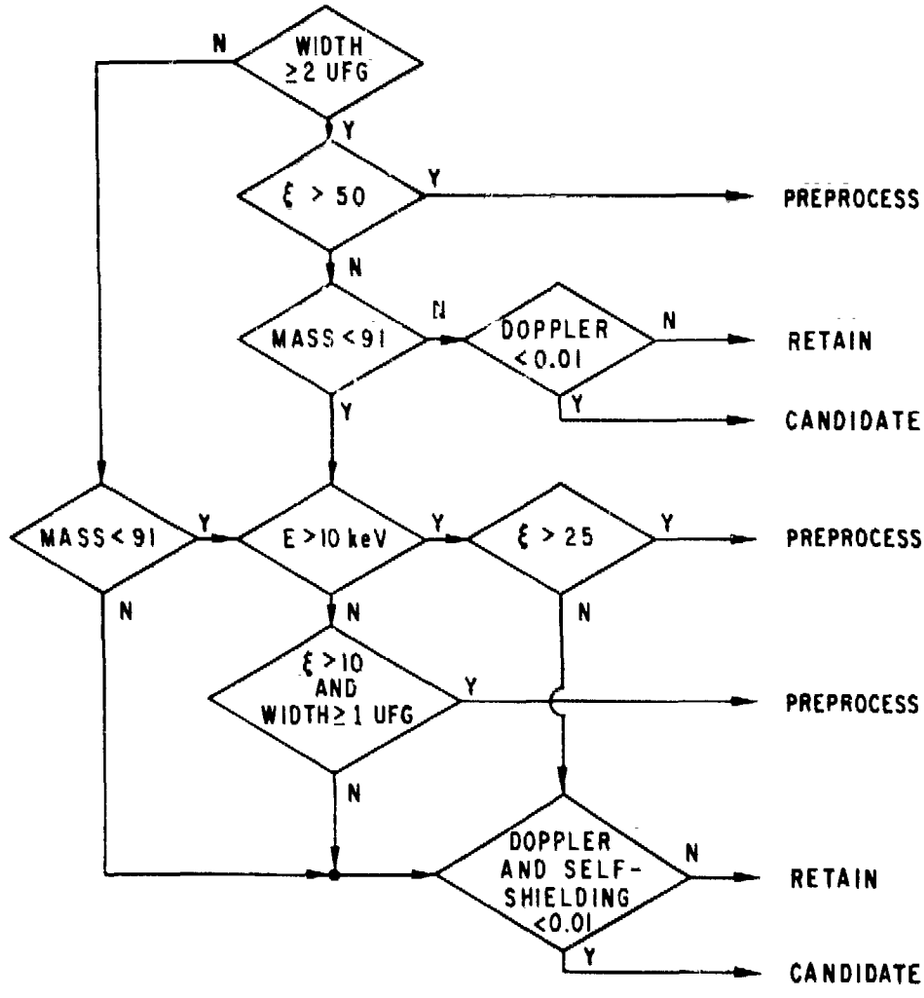

Fig. 1. Resonance Screening Logic.

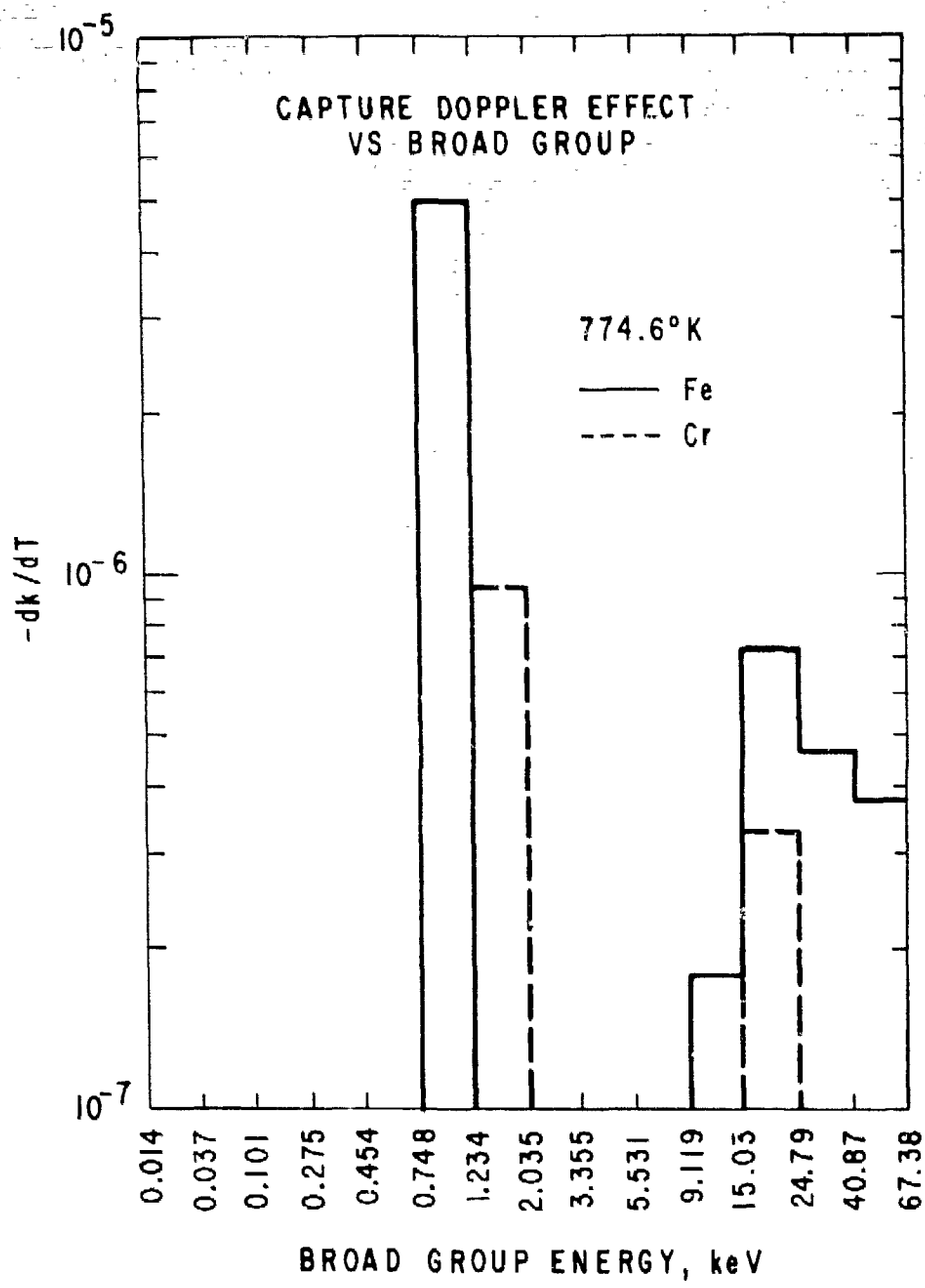

Fig. 2. Components of the Doppler Coefficient as a Function of Energy for Fe and Cr in the STF.

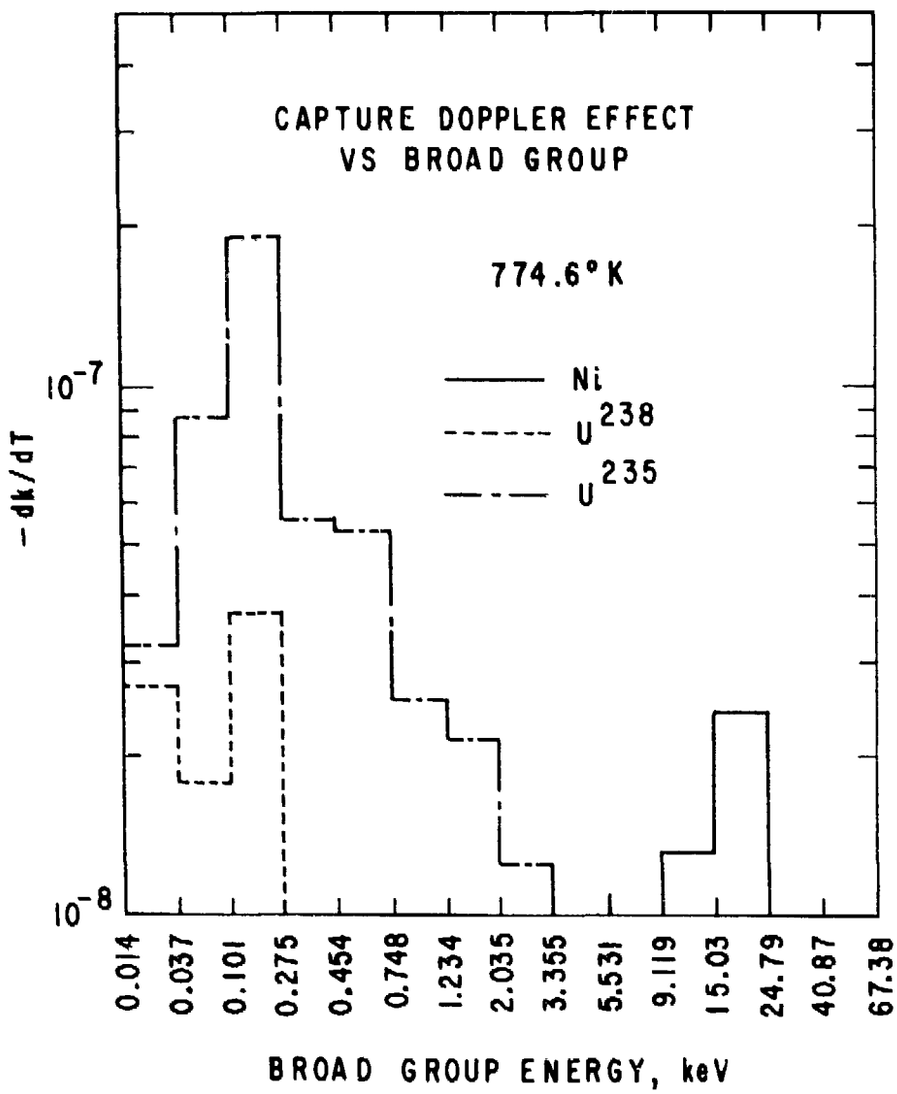

Fig. 3. Components of the Doppler Coefficient as a Function of Energy for Ni and ^{238}U and ^{235}U in the STF.

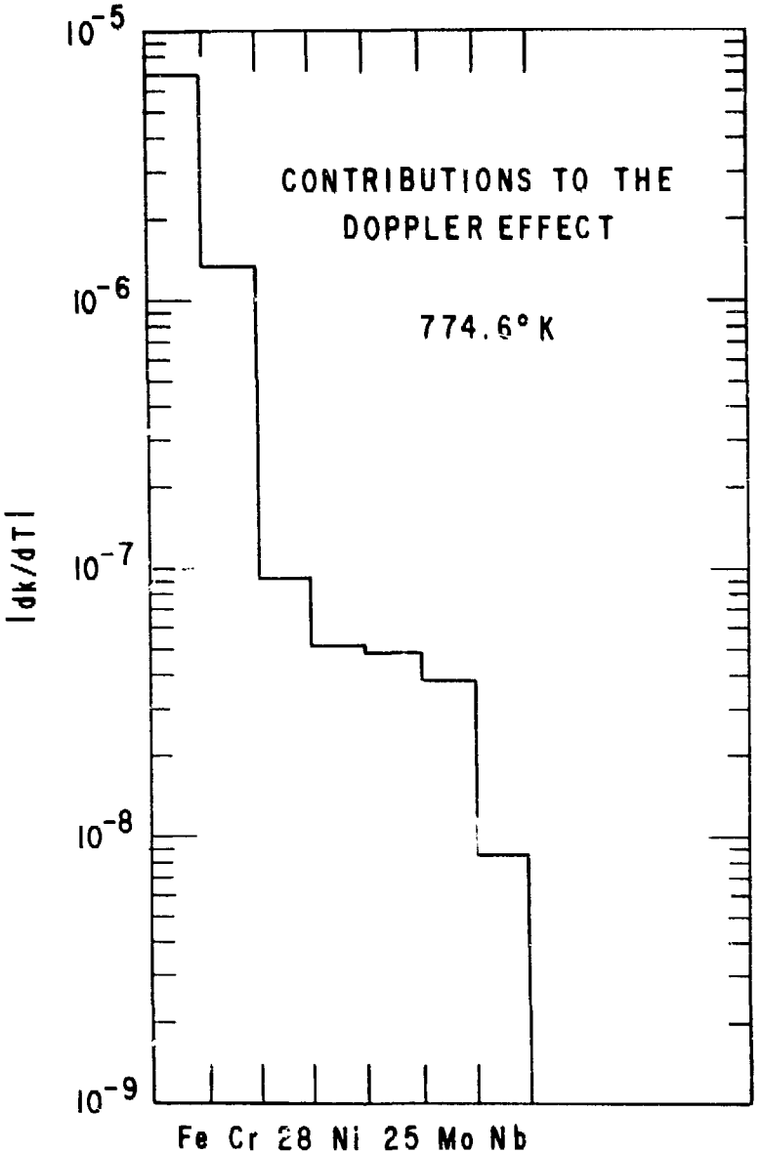

Fig. 4. Contributions from Each Nuclide to the Total Doppler Effect in the STF.

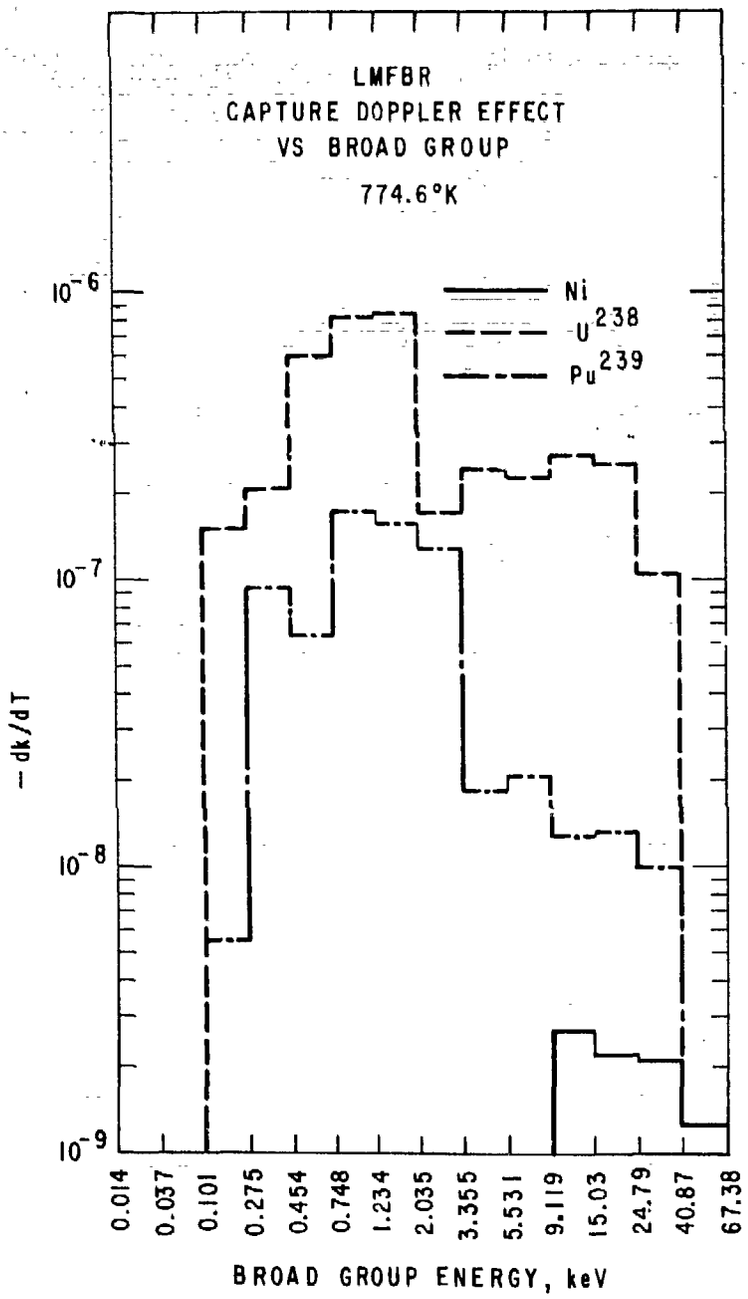

Fig. 5. Components of the Doppler Coefficient as a Function of Energy for Ni, ^{238}U, and ^{235}U in the LMFBR.

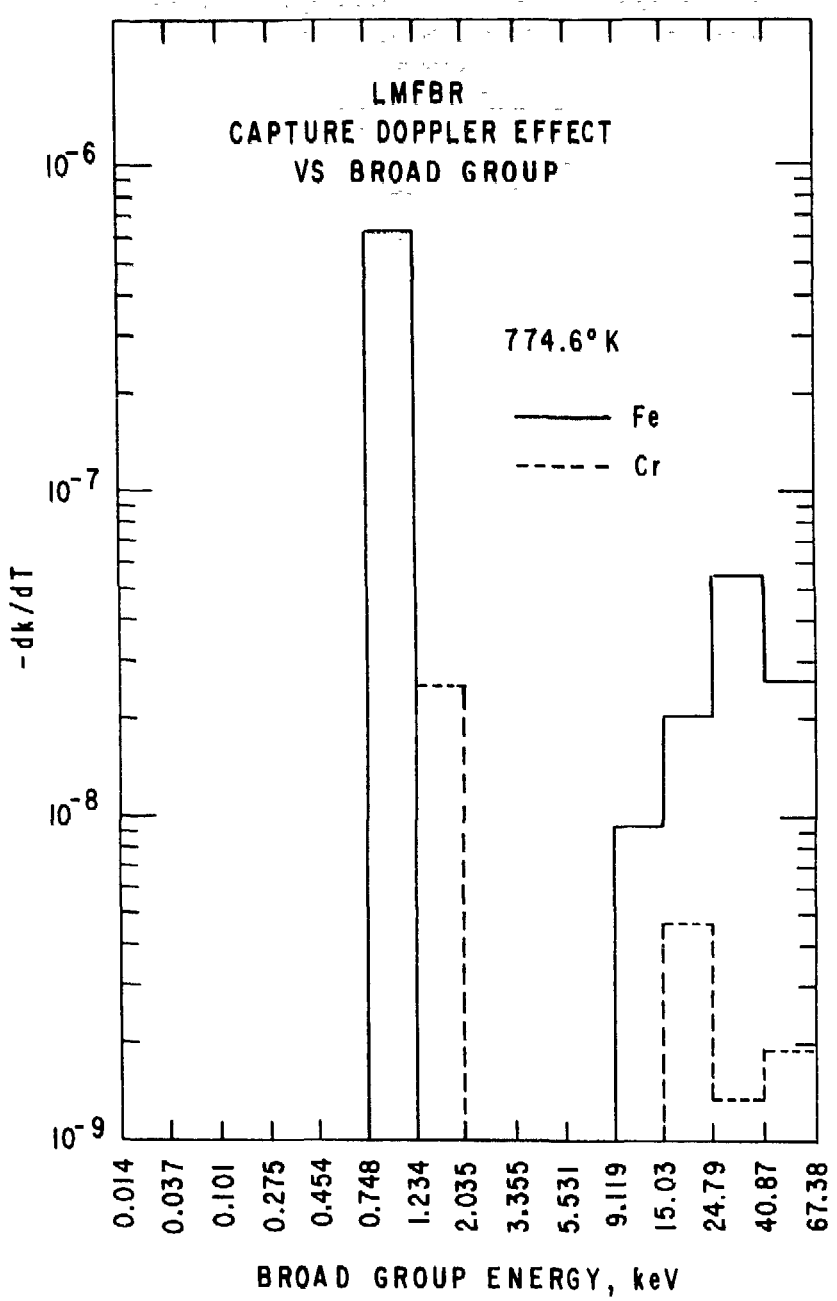

Fig. 6. Components of the Doppler Coefficient as a Function of Energy for Fe amd Cr in the LMFBR.

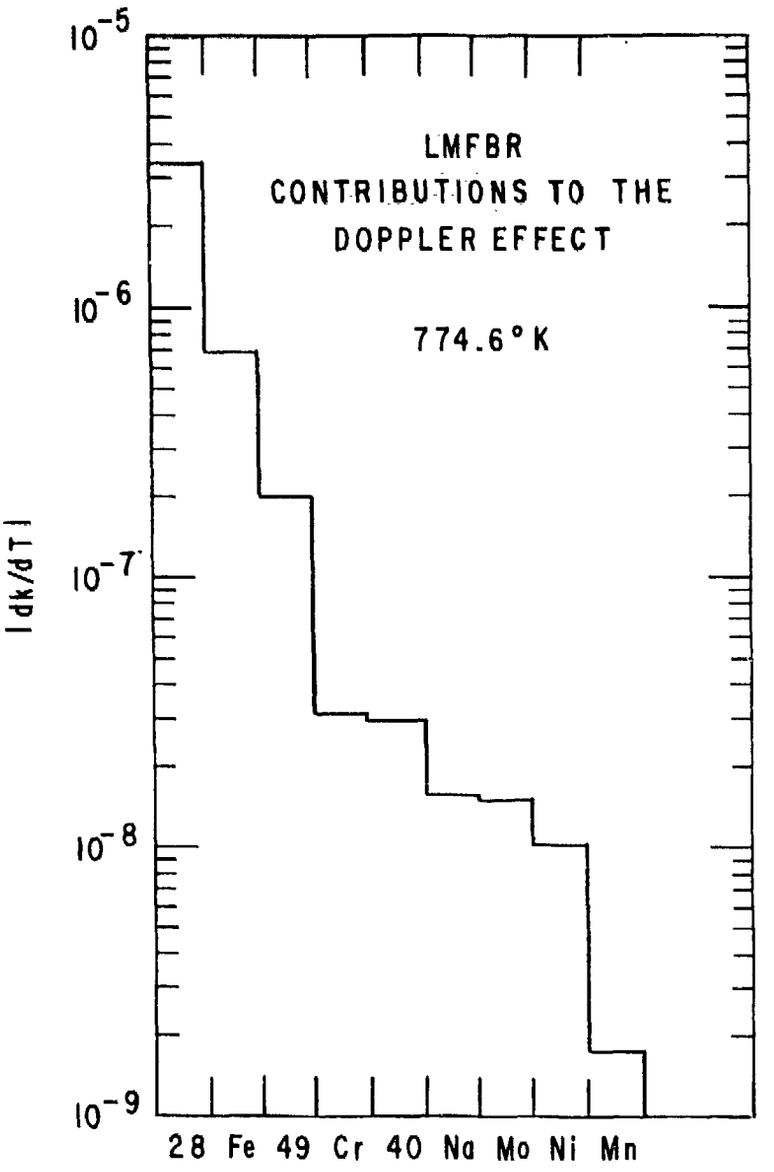

Fig. 7. Contributions from Each Nuclide to the Total Doppler Coefficient in the LMFBR.

TABLE I. Typical STF Converter Composition

Material	Atoms/cc × 10^{24}
Fe	4.9590×10^{-2}
Cr	1.1408×10^{-2}
O	1.7459×10^{-3}
Ni	1.6499×10^{-3}
^{235}U	8.1622×10^{-4}
^{238}U	5.6743×10^{-4}
Mo	1.5261×10^{-4}
Nb	6.3904×10^{-5}
Al	2.4118×10^{-5}
Mn	1.4803×10^{-5}
V	1.3584×10^{-5}

TABLE II. LMFBR Core Composition

Material	Atoms/cc × 10^{24}
Fe	1.9198×10^{-2}
O	1.174×10^{-2}
Na	8.8796×10^{-3}
^{238}U	5.135×10^{-3}
Cr	3.1986×10^{-3}
^{239}Pu	1.486×10^{-3}
Ni	1.476×10^{-3}
Mo	4.387×10^{-4}
Mn	2.428×10^{-4}
^{240}Pu	1.754×10^{-4}
^{241}Pu	1.62×10^{-5}
^{235}U	1.17×10^{-5}
^{241}Am	9.9×10^{-6}
^{242}Pu	2.1×10^{-6}

TABLE III. Broad Group Energy Structure and Resolved Resonance Ranges for Various Isotopes.

Broad Group	Upper Energy, eV	Resolved Resonance Range					
		Fe	Ni	Cr	^{238}U	^{235}U	^{239}Pu
1	10.0×10^6						
2	6.065×10^6						
3	3.679×10^6						
4	2.231×10^6						
5	1.353×10^6						
6	8.208×10^5						
7	4.979×10^5						
8	3.020×10^5						
9	1.832×10^5						
10	1.111×10^5						
11	6.738×10^4						
12	4.087×10^4						
13	2.479×10^4						
14	1.503×10^4						
15	9.119×10^3						
16	5.531×10^3						
17	3.355×10^3						
18	2.035×10^3						
19	1.234×10^3						
20	7.485×10^2						
21	4.540×10^2						
22	2.754×10^2						
23	1.013×10^2						
24	3.730×10^1						
25	1.370×10^1						
26	5.040×10^0						

TABLE IV. Some Interesting Statistics in the RABANL Calculation for the Typical LMFBR at T = 300°K[a]

Energy Span	1.5×10^5 - 1.85eV	4.0×10^3 - 1.85eV	3.0×10^2 - 1.85 eV
Total Number of hfg	112500	28233	8130
Total Number of Resonances			
1. Unscreened	1516	991	406
2. Screened	1085	874	359

[a]Default values of 4 hfg/Δ_{min} or 10 hfg/ε_{min} whichever is smaller.

TABLE V.- Capture Cross Sections at 300°K for Fe, Cr and Ni in the STF Converter

Broad Group	$\tilde{\sigma}_\gamma$, 300°K					
	Fe		Cr		Ni	
	Original	Improved	Original	Improved	Original	Improved
9	0.00548	0.00547	0.00598	0.00598	0.01554	0.01552
10	0.00878	0.00878	0.00874	0.00873	0.01730	0.01729
11	0.00609	0.00607	0.01377	0.01374	0.02359	0.02356
12	0.01196	0.01198	0.02714	0.02709	0.03127	0.03132
13	0.00489	0.00489	0.03233	0.03232	0.05166	0.05162
14	0.00845	0.00844	0.03115	0.03115	0.10775	0.10771
15	0.02425	0.02425	0.08519	0.08518	0.02095	0.02094
16	0.00751	0.00751	0.06382	0.06382	0.03457	0.03457
17	0.00538	0.00538	0.02551	0.02551	0.04730	0.04730
18	0.01062	0.01062	0.15196	0.15194	0.02211	0.02211
19	0.14296	0.14295	0.01974	0.01974	0.02493	0.02493
20	0.01654	0.01654	0.02293	0.02293	0.03102	0.03102
21	0.02151	0.02151	0.02795	0.02795	0.03920	0.03920
22	0.03031	0.03031	0.03800	0.03800	0.05466	0.05466
23	0.04881	0.04881	0.05988	0.05988	0.08746	0.08746
24	0.07867	0.07867	0.09574	0.09574	0.14062	0.14062
25	0.12690	0.12690	0.15395	0.15396	0.22663	0.22663
26	0.22097	0.22097	0.26775	0.26776	0.39446	0.39445

TABLE VI. Capture Cross Sections for ^{238}U and Fission Cross Sections for ^{235}U at 300°K in the STF Converter

	$\tilde{\sigma}_\gamma$, 300°K		$\tilde{\sigma}_f$, 300°K	
	^{238}U		^{235}U	
	Original	Improved	Original	Improved
15	0.81818	0.81818	3.3259	3.3259
16	1.0274	1.0275	4.2612	4.2612
17	1.3373	1.3374	5.2047	5.2046
18	1.7249	1.7249	6.8457	6.8456
19	2.6648	2.6646	8.3842	8.3841
20	3.4861	3.4860	13.072	13.072
21	3.4431	3.4431	13.486	13.486
22	12.232	12.231	20.419	20.419
23	12.829	12.829	29.247	29.247
24	116.24	116.24	47.034	47.034
25	38.701	38.701	45.382	45.382
26	0.81769	0.81769	15.300	15.300

TABLE VII. Total Cross Sections at 300°K for Fe, Cr and Ni in the STF Converter

Broad Group	$\tilde{\sigma}_t$, 300°K					
	Fe		Cr		Ni	
	Original	Improved	Original	Improved	Original	Improved
9	2.4865	2.4880	4.7699	4.7689	5.2425	5.2471
10	3.6495	3.6489	4.8936	4.8909	7.4993	7.4961
11	4.4747	4.4741	4.7675	4.7676	8.6899	8.6828
12	7.6397	7.6414	2.7684	2.7689	10.509	10.508
13	1.1934	1.1927	2.9794	2.9789	29.031	29.031
14	3.9054	3.9052	5.8214	5.8210	34.389	34.377
15	11.362	11.361	24.272	24.269	12.099	12.098
16	6.1950	6.1949	25.651	25.652	26.430	26.430
17	7.0179	7.0180	9.8901	9.8901	16.439	16.439
18	8.3896	8.3897	5.9892	5.9891	15.999	15.999
19	9.4450	9.4448	4.9575	4.9576	16.578	16.578
20	10.187	10.187	4.6523	4.6524	17.055	17.055
21	10.863	10.863	4.5225	4.5225	17.383	17.382
22	11.293	11.293	4.4529	4.4529	17.639	17.639
23	11.444	11.444	4.4267	4.4267	17.839	17.839
24	11.475	11.475	4.4465	4.4465	17.960	17.960
25	11.524	11.524	4.4987	4.4987	18.072	18.072
26	11.618	11.619	4.6103	4.6104	18.251	18.251

TABLE VIII. Comparison of IBM 370/195 CPU RABANL Execution Times for Original and Improved Algorithms for the STF Converter Composition Including All Resonances[a]

	CPU Times, Seconds	
	Original	Improved
Resonance Calc.	2660	325
Total Calc.	2870	500

[a]Based on default values of hfg.

TABLE IX. Capture Cross Sections for Structural Materials for the STF Converter Calculated by Using Unscreened and Screened Data[a]

	$\tilde{\sigma}_\gamma \times 10^3$, 300°K					
	Fe		Cr		Ni	
Broad Group	All Resonances	Screened	All Resonances	Screened	All Resonances	Screened
9	5.4750	5.4751	5.9821	6.0003	15.5308	15.5350
10	8.7794	8.7792	8.7303	8.7368	17.2974	17.3097
11	6.0663	6.1474	13.7378	13.7841	23.5668	23.6193
12	11.9631	11.9388	27.1415	27.1516	31.2720	31.2056
13	4.7311	4.7412	32.0036	32.0027	52.5569	52.5612
14	8.5148	8.5232	31.2219	31.2217	106.170	106.223
15	24.1710	24.1746	85.9023	85.9131	21.0138	21.0316
16	7.5296	7.5344	63.4118	63.4186	34.4238	34.4155
17	5.4170	5.4173	25.3069	25.3079	48.5220	48.5267
18	10.6743	10.6743	150.372	150.373	22.2717	22.2715
19	131.179	131.178	19.7860	19.7851	25.0446	25.0439
20	16.6543	16.6542	23.0413	23.0404	31.2144	31.2133
21	21.6563	21.6564	28.1106	28.1096	39.4566	39.4555
22	31.5910	31.5911	39.4984	39.4968	56.9198	56.9186
23	49.0726	49.0744	60.1965	60.1968	87.9267	87.9280
24	78.6675	78.6676	95.7373	95.7334	140.624	140.621
25	126.937	126.939	154.004	154.001	226.701	226.700
26	220.885	220.922	267.653	267.688	394.326	394.381

[a]Unresolved resonances ignored.

TABLE X. Capture of ^{238}U and Fission of ^{235}U for the STF Converter by Using Unscreened and Screened Data[a]

	$\tilde{\sigma}_\gamma$, 300°K		$\tilde{\sigma}_f$, 300°K	
	^{238}U		^{235}U	
Broad Group	All Resonances	Screened	All Resonances	Screened
16	0.39962	0.39951	0	0
17	1.3401	1.3401	0	0
18	1.7284	1.7285	0	0
19	2.6648	2.6654	0	0
20	3.4737	3.4737	0	0
21	3.4661	3.4661	0	0
22	14.5161	14.5161	0	0
23	13.2450	13.2477	21.7470	21.7333
24	116.233	116.243	47.0355	47.0422
25	38.8744	38.8871	45.3794	45.3660
26	0.81853	0.81822	15.2930	15.1865

[a]Unresolved resonances ignored.

TABLE XI. Doppler Changes in Capture Cross Sections for Structural Materials in the STF Obtained by Using Unscreened and Screened Data[a]

	$\Delta\tilde{\sigma}_\gamma \times 10^6$, 776-300°K					
	Fe		Cr		Ni	
Broad Group	All Resonances	Screened	All Resonances	Screened	All Resonances	Screened
9	3.3	3.2	24	24	3.9	3.2
10	6.0	6.0	20	20	7	7
11	331	320	184	148	99	101
12	581	587	38	75	167	152
13	403	400	813	812	384	390
14	267	267	39	39	624	600
15	4.1	10	27	27	208	209
16	2.7	2.2	32	28	-145	-144
17	2.6	2.6	0	0	172	170
18	-138	-138	15436	15436	-3.4	-3.5
19	22568	22571	-1	-1	-5	-5
20	1.5	1.7	-1	-1	1	1
21	1.9	1.9	-1	-1	1	1
22	-1.5	-1.5	-2	-2	6.2	3.8
23	-39	-39	-48	48	-73	-73
24	-208	-208	-252	-251	-372	-372
25	-550	-550	-664	-664	-980	-980
26	-39	-39	-48	-48	-49	-48

[a]Unresolved resonances ignored.

TABLE XII. Doppler Changes in Capture of ^{238}U and Fission of ^{235}U for the STF Obtained by Using Unscreened and Screened data[a]

	$\Delta\tilde{\sigma}_\gamma \times 10^6$, 774-300°K		$\Delta\tilde{\sigma}_f \times 10^6$, 774-300°K	
	^{238}U		^{235}U	
Broad Group	All Resonances	Screened	All Resonances	Screened
15	0	0	-	-
16	1927	1957	-	-
17	1900	1910	-	-
18	4160	4120	-	-
19	19340	19130	-	-
20	25590	25620	-	-
21	36780	36820	-	-
22	698000	698100	-	-
23	771900	772400	247000	248000
24	1566100	1563200	1658000	1624700
25	687000	687700	2250700	2250200
26	914	911	80500	78100

[a]Unresolved resonances ignored.

TABLE XIII. Capture Cross Sections for Structural Materials in the LMFBR the Obtained by Using Unscreened and Screened Data[a]

	$\tilde{\sigma}_\gamma \times 10^3$, 300°K					
	Fe		Cr		Ni	
Broad Group	All Resonances	Screened	All Resonances	Screened	All Resonances	Screened
9	5.4885	5.4881	6.4871	6.5070	14.3945	14.4111
10	8.7512	8.7511	9.5520	9.5569	17.0397	17.0563
11	6.1944	6.1918	14.7474	14.7751	23.6429	23.6578
12	14.9194	14.9010	28.8391	28.7512	36.8480	36.7810
13	5.0133	5.0159	33.3005	33.3036	58.8427	58.8454
14	9.4293	9.4326	31.5622	31.5618	100.807	100.843
15	25.4312	25.4367	85 9827	85.9842	20.7186	20.7253
16	7.6094	7.6147	67.7004	67.7084	36.2036	36.2024
17	5.8512	5.8563	23.3886	23.3886	66.9091	66.9817
18	11.1820	11.1833	189.749	189.825	22.5268	22.5255
19	179.358	179.405	19.7741	19.7738	25.0190	25.0184
20	16.5783	16.5784	22.9656	22.9646	31.0860	31.0852
21	21.4126	21.4124	27.8399	27.8387	39.0235	39.0225
22	28.8320	28.8314	36.2803	36.2783	52.0274	52.0239
23	44.7258	44.7250	55.0041	55.0008	80.1957	80.1926
24	76.5094	76.5061	93.1094	93.1029	136.741	136.735
25	124.305	120.206	150.825	150.701	222.015	221.833
26	232.961	232.988	282.256	282.282	415.870	415.909

[a]Unresolved resonances ignored.

TABLE XIV. Capture of ^{238}U and Fission of ^{239}Pu in the LMFBR Obtained by Using Unscreened and Screened Data[a]

	$\tilde{\sigma}_\gamma$, 300°K		$\tilde{\sigma}_f$, 300°K	
	^{238}U		^{235}Pu	
Broad Group	All Resonances	Screened	All Resonances	Screened
16	0.219844	0.219908	-	-
17	1.13628	1.13723	-	-
18	1.04163	1.04084	-	-
19	1.31976	1.32125	-	-
20	1.43651	1.43638	-	-
21	1.47469	1.47454	2.34497	2.34061
22	2.20767	2.20756	14.8994	14.9101
23	2.14631	2.14857	34.7200	34.7259
24	10.1100	10.1117	11.1377	11.1319
25	2.55074	2.51892	38.8079	38.8406
26	0.711772	0.711644	11.4720	11.4090

[a]Unresolved resonances ignored.

TABLE XV. Doppler Changes in Capture Cross Sections of Structural Materials in the LMFBR Obtained by Using Unscreened and Screened Data[a]

	$\Delta\tilde{\sigma}_\gamma \times 10^6$, 776°K-300°K					
	Fe		Cr		Ni	
Broad Group	All Resonances	Screened	All Resonances	Screened	All Resonances	Screened
9	5.07	5.48	17.3	17.4	11.9	10.8
10	7.34	7.88	21.2	20.0	11.5	10.8
11	172.06	164.9	100.8	84.8	98.8	100.2
12	486.3	488.2	1.0	87.4	294.6	280.8
13	184.8	183.4	290.4	288.5	231.3	238.5
14	146.8	146.1	32.5	31.6	480	466
15	2.4	7.5	17.4	22.2	196	195.8
16	1.8	1.0	84.1	81.3	-230	-230.7
17	-9	14	8.7	9.1	246.3	239.3
18	-40.3	-40.5	5160	5138	-5.4	-4.5
19	32426	32418.	-5.2	-5.8	-15.1	-15.2
20	-10.6	-10.9	-12.3	-12.4	-24.7	-24.5
21	-17.1	-16.9	-15.4	-15.2	-23.0	-23.1
22	-162.4	-162.3	-188.7	-188.6	-268.1	-266.4
23	-252.5	-251.0	-300.5	-299.2	-446.8	-444.6
24	-138.2	-141.0	-142.8	-146.7	-213.0	-221.0
25	3761	3743	4541	4517	6673	6641
26	261	264	318	320	466	474

[a]Unresolved resonances ignored.

TABLE XVI. Doppler Changes in Capture of ^{238}U and Fission of ^{239}Pu in the LMFBR Obtained by Using Unscreened and Screened Data[a]

	$\Delta\tilde{\sigma}_\gamma \times 10^6$, 776°K-300°K		$\Delta\tilde{\sigma}_f \times 10^6$, 776°K-300°K	
	^{238}U		^{239}Pu	
Broad Group	All Resonances	Screened	All Resonances	Screened
15	0	0	0	0
16	13649	13488	0	0
17	68880	67840	0	0
18	118810	118640	0	0
19	202870	202260	0	0
20	282900	282830	0	0
21	299790	299520	21950	230400
22	432330	432460	682400	679500
23	339380	339210	568500	536700
24	1003500	1005600	649400	642500
25	1216390	1210110	248000	252000
26	-1914	-1950	21500	21400

[a]Unresolved resonances ignored.

TABLE XVII. Comparison of IBM 370/195 CPU Execution Times of RABANL for Cases With and Without Resonance Data Preprocessing[a]

	CPU Times, Seconds			
	STF		LMFBR	
	No Preprocessing	Preprocessing	No Preprocessing	Preprocessing
Resonance Calc.	325	245	389	246
Total Calc.	500	420	676	525

[a]Default values of hfg.

TABLE XVIII. Total and Capture Cross Sections of Fe at 300°K as Obtained by Various Methods

Broad Group	$\bar{\sigma}_t$, 300°K				$\bar{\sigma}_\gamma$, 300°K			
	VIM	RABANL	NRA	Improved NRA	VIM	RABANL	NRA	Improved NRA
9	2.410 ± 0.07%	2.4871	2.5064	2.5043	0.00548 ± 0.004%	0.005475	0.005485	0.005485
10	3.596 ± 0.07%	3.6492	3.7099	3.7061	0.00879 ± 0.005%	0.008779	0.008789	0.008789
11	4.484 ± 0.02%	4.4761	4.4825	4.4819	0.00639 ± 0.76%	0.006150	0.006138	0.006135
12	7.653 ± 0.08%	7.6465	7.6769	7.6705	0.01202 ± 0.72%	0.01196	0.01200	0.01199
13	1.192 ± 0.04%	1.1923	1.1896	1.1899	0.00506 ± 0.72%	0.004900	0.004881	0.004882
14	3.908 ± 0.02%	3.9048	3.9061	3.9062	0.00842 ± 0.75%	0.008452	0.008452	0.008443
15	11.377 ± 0.02%	11.3632	11.372	11.3720	0.02434 ± 0.08%	0.02425	0.02430	0.02430
16	6.204 ± 0.009%	6.1948	6.1979	6.1979	0.00753 ± 0.1%	0.007513	0.007519	0.007519
17	7.023 ± 0.004%	7.0173	7.0195	7.0195	0.00544 ± 0.12%	0.005380	0.005360	0.005360
18	8.394 ± 0.003%	8.3890	8.3917	8.3920	0.01078 ± 0.31%	0.01062	0.010230	0.01022
19	9.449 ± 0.01%	9.4449	9.4556	9.4477	0.14236 ± 0.82%	0.14289	0.14759	0.14173
20	10.192 ± 0.002%	10.1869	10.190	10.190	0.01654 ± 0.008%	0.016538	0.01654	0.016539
21	10.865 ± 0.002%	10.8628	10.864	10.864	0.02154 ± 0.01%	0.021510	0.02151	0.021512
22	11.295 ± 0.002%	11.2929	11.295	11.294	0.03033 ± 0.04%	0.030312	0.03032	0.030322
23	11.448 ± 0.0004%	11.4438	11.448	11.448	0.04877 ± 0.08%	0.048811	0.04881	0.04882
24	11.479 ± 0.002%	11.4752	11.478	11.478	0.07862 ± 0.27%	0.078667	0.07906	0.07906
25	11.528 ± 0.01%	11.5252	11.524	11.527	0.12823 ± 0.15%	0.12695	0.12753	0.12753
26	11.619 ± 0.03%	11.6193	11.620	11.620	0.21940 ± 1.55%	0.22098	0.22146	0.22146

TABLE XIX. Capture of ^{238}U and Fission of ^{235}U at 300°K
for the STF as Obtained by Various Methods

Broad Group	^{238}U $\bar{\sigma}_\gamma$, 300°K VIM	RABANL	NRA	Improved NRA	^{235}U $\bar{\sigma}_f$, 300°K VIM	RABANL	NRA	Improved NRA
15	0.82010 ± 0.10%	0.81911	0.81924	0.81926	3.3384 ± 0.04%	3.3296	3.3313	3.3313
16	1.0312 ± 0.15%	1.02822	1.0250	1.02510	4.2706 ± 0.04%	4.2636	4.2656	4.2656
17	1.3405 ± 0.22%	1.3374	1.3412	1.3418	5.2052 ± 0.05%	5.2029	5.2046	5.2046
18	1.7301 ± 0.28%	1.7244	1.7246	1.7262	6.8598 ± 0.06%	6.8399	6.8420	6.8409
19	2.6672 ± 0.34%	2.6653	2.6599	2.6619	8.4256 ± 0.07%	8.3768	8.3759	8.3804
20	3.4743 ± 0.52%	3.4856	3.4857	3.4879	13.065 ± 0.08%	13.0608	13.065	13.0647
21	3.4358 ± 0.84%	3.4427	3.4139	3.4171	13.493 ± 0.1%	13.4712	13.474	13.474
22	12.204 ± 0.91%	12.2354	12.1130	12.2483	20.462 ± 0.12%	20.3740	20.384	20.384
23	12.722 ± 2.32%	12.8327	12.4014	12.5274	29.319 ± 0.29%	29.2040	29.578	29.441
24	113.01 ± 4.21%	116.251	114.158	114.158	46.684 ± 1.17%	47.0410	48.773	48.772
25	22.333 ± 23.2%	38.9267	44.135	44.1346	45.420 ± 4.88%	45.3624	46.207	46.207
26	0.84077 ± 4.94%	0.81767	0.01439	0.014395	15.650 ± 5.15%	15.1913	15.282	15.282

TABLE XX. Doppler Changes $\Delta\tilde{\sigma}_\gamma$ for Fe in the STF at Two Temperature Ranges as Obtained by Various Methods

Broad Group	$\Delta\tilde{\sigma}_\gamma \times 10^6$, 776-300°K			$\Delta\tilde{\sigma}_\gamma \times 10^6$, 2000-776°K		
	RABANL	NRA	Improved NRA	RABANL	NRA	Improved NRA
9	0	0	0	0	0	0
10	0	0	0	0	0	0
11	319	317	317	254	252	252
12	589	597	595	490	496	495
13	414	416	416	410	415	413
14	262	265	264	206	207	207
15	11	11	11	9	9	9
16	3	1	1	4	1	1
17	4	1	1	7	1	1
18	-134	-139	-139	-22	-25	-25
19	24849	26380	24056	38485	40825	36740
20	0	0	0	0	0	0
21	-1	-1	0	0	0	0
22	-13	-17	-17	-11	-14	-14
23	-40	-46	-46	-46	-57	-40
24	-208	-148	-148	-255	-173	-174
25	-548	-442	-442	-509	-490	-490
26	-13	-28	-28	-8	-29	-29

TABLE XXI. Doppler Changes $\Delta\tilde{\sigma}_\gamma$ for Cr in the STF at Two Temperature Ranges as Obtained by Various Methods

Broad Group	$\Delta\tilde{\sigma}_\gamma \times 10^6$, 776-300°K			$\Delta\tilde{\sigma}_\gamma \times 10^6$, 2000-776°K		
	RABANL	NRA	Improved NRA	RABANL	NRA	Improved NRA
9	23.6	21.8	21.8	22.9	18	18
10	19.6	12.4	12.4	16.9	8.3	8.3
11	147.9	138.7	138.9	145.8	133.5	134
12	77.4	104.1	104.2	-14.4	80	80
13	844.4	829	825.3	852.6	821	817
14	53	28.8	28.7	23.4	21.4	21.4
15	3	0	0	2.0	0	0
16	0	0	0	0	0	0
17	0	0	0	1.0	0	0
18	15461	15808	15364	15552	15937	15434
19	0	0	0	0	0	0
20	0	0	0	0	0	0
21	-1	-1	-1	0	0	0
22	-15.4	-20	-20	-13.5	-16.1	-16.1
23	-51.2	-54.5	-54.6	-53.1	-47.2	-47.3
24	-250	-179	-179	-307	-209	-209
25	-663	-535	-535	-615	-591	-591
26	-15	-34	-51	-10	-35	-36

TABLE XXII. Doppler Changes $\Delta\tilde{\sigma}_\gamma$ for Ni in the STF at Two Temperature Ranges as Obtained by Various Methods

Broad Group	$\Delta\tilde{\sigma}_\gamma \times 10^6$, 776-300°K			$\Delta\tilde{\sigma}_\gamma \times 10^6$, 2000-776°K		
	RABANL	NRA	Improved NRA	RABANL	NRA	Improved NRA
9	3.2	1.0	1.0	7.3	1.0	1.0
10	7.4	0	0	3.2	0	0
11	100.6	90.9	90.9	83.6	74.7	75.0
12	154.2	138.5	139.7	116.3	102.4	103.5
13	391.6	407.9	405.3	434.6	458.8	456
14	608.0	606.0	606.0	431.0	434.0	434
15	204.3	2.1	2.1	136.3	1.0	1.0
16	-165.3	3.7	3.6	-111.0	2.3	2.3
17	143.3	145.3	145.6	111.8	110.8	110.8
18	-2.5	-3.5	-3.8	0	0	0
19	-1.6	-4.2	-5.0	-3	-12	-12
20	7.3	0	0	-1	-1.0	-1.0
21	-2	-2	-2	0	-1.0	-1.0
22	-23.1	-30	-30	-20.8	-24.3	-24.3
23	-79.7	-81.1	-81.5	-88.8	-70.3	-70.1
24	-371	-264	-264	-454	-308	-309
25	-977	-790	-790	-900	-872	-872
26	-20	-51	-49	-13	-52	-53

TABLE XXIII. Total and Capture Cross Sections for Fe at 300°K in the LMFBR as Obtained by Various Methods

Broad Group	$\bar{\sigma}_t$, 300°K				$\bar{\sigma}_\gamma$, 300°K			
	VIM	RABANL	NRA	Improved NRA	VIM	RABANL	NRA	Improved NRA
9	3.046 ± 0.07%	3.1111	3.1152	3.1147	0.0055 ± 0.005%	0.005488	0.005495	0.005495
10	4.372 ± 0.06%	4.4177	4.4319	4.4316	0.0088 ± 0.007%	0.008750	0.008764	0.008764
11	4.527 ± 0.02%	4.5246	4.5271	4.5269	0.0065 ± 0.84%	0.006225	0.006204	0.006202
12	10.958 ± 0.08%	10.9505	11.0225	11.0239	0.0149 ± 0.75%	0.014989	0.014975	0.014971
13	1.351 ± 0.06%	1.3488	1.3506	1.3517	0.0055 ± 1.37%	0.005275	0.005315	0.005277
14	3.998 ± 0.04%	3.9934	3.9976	3.9976	0.0094 ± 0.90%	0.009265	0.009237	0.009235
15	11.883 ± 0.05%	11.8749	11.8975	11.8976	0.0258 ± 0.14%	0.025767	0.025807	0.025807
16	6.118 ± 0.02%	6.1062	6.1083	6.1100	0.0076 ± 0.18%	0.007554	0.007552	0.007556
17	7.259 ± 0.01%	7.2554	7.2577	7.2583	0.0059 ± 0.32%	0.005848	0.005823	0.005825
18	3.424 ± 0.01%	8.4200	8.4248	8.4236	0.0113 ± 0.65%	0.011157	0.010769	0.010779
19	9.508 ± 0.04%	9.5078	9.5139	9.5024	0.2066 ± 1.72%	0.20899	0.21036	0.200954
20	10.157 ± 0.01%	10.1498	10.1553	10.1553	0.0164 ± 0.04%	0.016347	0.016364	0.016363
21	10.838 ± 0.01%	10.8360	10.8368	10.8371	0.0213 ± 0.05%	0.021236	0.021241	0.021245
22	11.264 ± 0.02%	11.2566	11.2635	11.2635	0.0289 ± 0.25%	0.028784	0.028949	0.028949
23	11.444 ± 0.004%	11.4382	11.4437	11.4436	0.0448 ± 0.82%	0.044720	0.045107	0.045052
24	---	11.4753	11.4766	11.4766	---	0.077495	0.077268	0.077268
25	---	11.5319	11.5314	11.5315	---	0.133520	0.131956	0.131960
26	---	11.6325	11.6325	11.6325	---	0.233182	0.23298	0.23298

TABLE XXIV. Capture of ^{238}U and Fission of ^{239}Pu at 300°K for the LMFBR as Obtained by Various Methods

Broad Group	^{238}U $\tilde{\sigma}_\gamma$, 300°K				^{239}Pu $\tilde{\sigma}_f$, 300°K			
	VIM	RABANL	NRA	Improved NRA	VIM	RABANL	NRA	Improved NRA
15	0.7456 ± 0.12%	0.7446	0.7447	0.7447	2.072 ± 0.07%	2.0687	2.0707	2.0707
16	0.8685 ± 0.18%	0.8721	0.8696	0 .8715	2.394 ± 0.10%	2.3939	2 3941	2.3953
17	1.150 ± 0.43%	1.1436	1.1387	1.1488	3.032 ± 0.15%	3.0145	3.0150	3.0142
18	1.059 ± 0.39%	1.0503	1.0387	1.0495	3.922 ± 0.21%	3.8965	3.9193	3.9139
19	1.348 ± 0.67%	1.3457	1.3180	1.3332	5.773 ± 0.26%	5.7121	5.6986	5.7009
20	1.478 ± 1.11%	1.4828	1.4250	1.4327	7.572 ± 0.45%	7.4594	7.4794	7.4824
21	1.467 ± 2.25%	1.4965	1.4304	1.4343	8.646 ± 0.74%	8.5296	8.5727	8.5753
22	2.338 ± 2.72%	2.2098	2.0237	2.1203	14.909 ± 1.15%	14.9331	14.7546	14.7069
23	1.775 ± 12.9%	2.1470	1.5078	1.5825	36.009 ± 4.02%	34.6858	34.9951	34.5618
24	---	9.5810	10.4597	10.6787	---	12.8557	12.5388	10.8730
25	---	5.1893	6.8485	6.8851	---	35.9731	45.6468	36.7859
26	---	0.7099	0.01527	0.01527	---	11.4249	10.5245	10.5245

TABLE XXV. Doppler Changes $\Delta\tilde{\sigma}_\gamma$ for Fe in the LMFBR at Two Temperature Ranges as Obtained by Various Methods

Broad Group	$\Delta\tilde{\sigma}_\gamma \times 10^6$, 776-300°K			$\Delta\tilde{\sigma}_\gamma \times 10^6$, 2000-776°K		
	RABANL	NRA	Improved NRA	RABANL	NRA	Improved NRA
9	-	-	-	-	-	-
10	-	-	-	-	-	-
11	165.6	163.88	163.83	120.1	117.87	117.83
12	485.3	496.5	495.5	370.0	381.2	380.5
13	185.6	205.2	201.9	141.1	157.66	155.27
14	134.3	137.9	137.8	96.6	103.83	103.72
15	13.6	9.4	9.5	12.0	11.1	11.1
16	4.5	-2.4	-2.1	-1.0	-1.8	-1.63
17	-13.8	-13.9	-14.2	-7.7	-8.8	-9.12
18	-40.9	-89.6	-88.3	-52.5	-82.0	-80.2
19	38372.0	43626.0	39254.0	49885	55252	48611.0
20	-21.7	-18.7	-21.7	-19.8	-17.0	-17.0
21	-19.7	-24.0	-23.8	-24.7	-23.0	-22.6
22	-158.3	-114.3	-114.7	-190.6	-128.7	-127.8
23	-230.0	-186.9	-193.4	-289.7	-230.8	-244.0
24	616.3	175.7	175.5	1098.0	413.6	413.6
25	1454.0	1776.0	1776.0	877.0	1295.9	1259.0
26	130.0	77.0	77.0	264.0	112.0	112.0

TABLE XXVI. Doppler Changes $\Delta\tilde{\sigma}_\gamma$ for ^{238}U in the LMFBR at Two Temperature Ranges as Obtained by Various Methods

Broad Group	$\Delta\tilde{\sigma}_\gamma \times 10^6$, 776-300°K			$\Delta\tilde{\sigma}_\gamma \times 10^6$, 2000-776°K		
	RABANL	NRA	Improved NRA	RABANL	NRA	Improved NRA
15	23496	23478	23478	17235	17209	17210
16	44850	44285	44724	35209	34701	35145
17	67140	67650	70650	60870	61680	65340
18	117460	113730	118400	123590	122580	129260
19	202050	197700	205460	227630	226980	238450
20	290210	276310	282180	339160	324070	334200
21	299470	289810	293800	339860	318910	326740
22	435130	358830	390700	701230	553520	619920
23	339060	258450	256010	56499	367290	380970
24	438390	248000	219100	649300	1285500	1335600
25	625530	1234810	1241280	759230	1497120	1504404
26	-773	5.8	5.6	-1370	8.5	8.5

TABLE XXVII. Doppler Changes $\Delta\tilde{\sigma}_f$ for ^{239}Pu in the LMFBR at Two Temperature Ranges as Obtained by Various Methods

Broad Group	$\Delta\tilde{\sigma}_f \times 10^6$, 776-300°K			$\Delta\tilde{\sigma}_f \times 10^6$, 2000-776°K		
	RABANL	NRA	Improved NRA	RABANL	NRA	Improved NRA
16[a]	8830	6350	6500	4950	4650	4780
17[a]	10890	11160	10990	8500	8910	8700
18[a]	53110	56590	55540	39490	44950	43780
19[a]	116230	114820	115040	93710	90800	91340
20[a]	140750	148900	150690	93100	102730	104990
21[a]	233180	247790	248250	206950	184900	185950
22	680400	541600	543000	665200	523700	497800
23	531500	600400	53880	445600	644100	452800
24	2112000	1178200	1178200	3926600	2117900	2117600
25	841100	326900	327200	2333000	2555600	2555800
26	10500	6200	6300	21500	9200	9100

[a]Unresolved region. Strictly speaking, comparison is not meaningful.

TABLE XXVIII. Components of $\Delta\tilde{\sigma}_\gamma$ for ^{238}U of the LMFBR in groups 17 and 18

774–300°K

Broad Group	RABANL			NRA			Improved NRA		
	$\tilde{\phi}$ 300°K	$\frac{\Delta R_\gamma}{\tilde{\phi}}$	$-\tilde{\sigma}_\gamma \frac{\Delta\tilde{\phi}}{\tilde{\phi}}$	$\tilde{\phi}$ 300°K	$\frac{\Delta R_\gamma}{\tilde{\phi}}$	$-\tilde{\sigma}_\gamma \frac{\Delta\tilde{\phi}}{\tilde{\phi}}$	$\tilde{\phi}$ 300°K	$\frac{\Delta R_\gamma}{\tilde{\phi}}$	$-\tilde{\sigma}_\gamma \frac{\Delta\tilde{\phi}}{\tilde{\phi}}$
17	0.99120	0.05084	0.01539	0.98548	0.04787	0.01867	0.99337	0.05198	0.01530
18	2.6584	0.08685	0.02754	2.6434	0.07925	0.03108	2.6692	0.08563	0.02806

2000–774°K

Broad Group	RABANL			NRA			Improved NRA		
	$\tilde{\phi}$ 300°K	$\frac{\Delta R_\gamma}{\tilde{\phi}}$	$-\tilde{\sigma}_\gamma \frac{\Delta\tilde{\phi}}{\tilde{\phi}}$	$\tilde{\phi}$ 300°K	$\frac{\Delta R_\gamma}{\tilde{\phi}}$	$-\tilde{\sigma}_\gamma \frac{\Delta\tilde{\phi}}{\tilde{\phi}}$	$\tilde{\phi}$ 300°K	$\frac{\Delta R_\gamma}{\tilde{\phi}}$	$-\tilde{\sigma}_\gamma \frac{\Delta\tilde{\phi}}{\tilde{\phi}}$
17	0.97643	0.04820	0.01215	0.96932	0.04461	0.01624	0.97817	0.04945	0.01509
18	2.5851	0.09434	0.02638	2.5643	0.08718	0.03199	2.5943	0.09591	0.03003

TABLE XXIX. Components of $\Delta\tilde{\sigma}_\gamma$ for ^{238}U of the STF in Group 19

774-300°K

	RABANL			NRA			Improved NRA		
Broad Group	$\tilde{\phi}$ 300°K	$\frac{\Delta R_\gamma}{\tilde{\phi}}$	$-\tilde{\sigma}_\gamma \frac{\Delta\tilde{\phi}}{\tilde{\phi}}$	$\tilde{\phi}$ 300°K	$\frac{\Delta R_\gamma}{\tilde{\phi}}$	$-\tilde{\sigma}_\gamma \frac{\Delta\tilde{\phi}}{\tilde{\phi}}$	$\tilde{\phi}$ 300°K	$\frac{\Delta R_\gamma}{\tilde{\phi}}$	$-\tilde{\sigma}_\gamma \frac{\Delta\tilde{\phi}}{\tilde{\phi}}$
19	3.4024	0.02018	0.003917	3.3097	0.02327	0.004303	3.3361	0.01939	0.003985

2000-774°K

	RABANL			NRA			Improved NRA		
Broad Group	$\tilde{\phi}$ 300°K	$\frac{\Delta R_\gamma}{\tilde{\phi}}$	$-\tilde{\sigma}_\gamma \frac{\Delta\tilde{\phi}}{\tilde{\phi}}$	$\tilde{\phi}$ 300°K	$\frac{\Delta R_\gamma}{\tilde{\phi}}$	$-\tilde{\sigma}_\gamma \frac{\Delta\tilde{\phi}}{\tilde{\phi}}$	$\tilde{\phi}$ 300°K	$\frac{\Delta R_\gamma}{\tilde{\phi}}$	$-\tilde{\sigma}_\gamma \frac{\Delta\tilde{\phi}}{\tilde{\phi}}$
19	3.3090	0.03066	0.006417	3.2132	0.03334	0.006058	3.2423	0.02977	0.006706